

Multi-platform Observations of Severe Typhoon Koinu

Junyi HE¹, Pak Wai Chan², Chun-Wing Choy², Ping Cheung², Y.W. Chan², C.C. Lam², Y.H. He², Pingping Rong³, Hui Su³, and Zhaoming Li⁴

¹City University of Hong Kong

²Hong Kong Observatory

³Hong Kong University of Science and Technology

⁴Foshan Tornado Research Center

November 8, 2023

Abstract

Severe Typhoon Koinu passed south of Hong Kong on 8 and 9 October 2023, triggering the issuance of the Increasing Gale or Storm Signal No. 9, the second highest tropical cyclone warning signal in Hong Kong. Koinu was a difficult case for TC warning service due to its compact size and rather erratic movement over coastal waters of Guangdong. To monitor Koinu's movement and wind structure, the Hong Kong Observatory utilized various observational platforms, including meteorological aircraft, ocean radar, and synthetic aperture radar on polar orbiting satellites. The paper presents major observations derived from these measurements. The aircraft probe and drosonde data suggested boundary layer inflow, warm core structure, eyewall updraft and downdraft, and high turbulence in the eyewall of the typhoon. The weather radar observations indicated occurrence of a waterspout in the vicinity of the typhoon. Additionally, the study evaluates the forecasting performance of the AI-based Pangu-Weather model, and the results highlight its better performance than the global numerical weather prediction models in forecasting tropical cyclones in the region. The documentation of these observations aims to provide valuable references for weather forecasters and stimulate further research on forecasting this type of tropical cyclones.

Hosted file

977173_0_art_file_11518593_s30856.docx available at <https://authorea.com/users/677947/articles/674793-multi-platform-observations-of-severe-typhoon-koinu>

1
2 **Multi-platform Observations of Severe Typhoon Koinu**

3
4 **J. Y. He¹, P. W. Chan^{2*}, C. W. Choy², P. Cheung², Y. W. Chan², C. C. Lam², Y. H. He², P.**
5 **Rong³, H. Su³, and Z. M. Li^{4,5}**

6
7 ¹City University of Hong Kong, Kowloon Tong, Hong Kong.

8 ²Hong Kong Observatory, Kowloon, Hong Kong.

9 ³Dept. of Civil and Environmental Engineering, The Hong Kong University of Science and
10 Technology, Clear Water Bay, Hong Kong

11 ⁴Foshan Tornado Research Center, Foshan, Guangdong, China.

12 ⁵China Meteorological Administration Tornado Key Laboratory, Foshan, Guangdong, China.

13
14 *Corresponding author: P. W. Chan (pwchan@hko.gov.hk)

15
16 **Key Points:**

- 17 • Observations from meteorological aircraft, ocean radar, and synthetic aperture radar show
18 the structure of Severe Typhoon Koinu.
- 19 • Weather radar observations suggest the occurrence of a waterspout in the vicinity of
20 Koinu.
- 21 • AI-based Pangu-Weather model outperforms the conventional global numerical weather
22 prediction models in forecasting Koinu.
- 23

24 **Abstract**

25 Severe Typhoon Koinu passed south of Hong Kong on 8 and 9 October 2023, triggering the
26 issuance of the Increasing Gale or Storm Signal No. 9, the second highest tropical cyclone
27 warning signal in Hong Kong. Koinu was a difficult case for TC warning service due to its
28 compact size and rather erratic movement over coastal waters of Guangdong. To monitor
29 Koinu's movement and wind structure, the Hong Kong Observatory utilized various
30 observational platforms, including meteorological aircraft, ocean radar, and synthetic aperture
31 radar on polar orbiting satellites. The paper presents major observations derived from these
32 measurements. The aircraft probe and drosonde data suggested boundary layer inflow, warm
33 core structure, eyewall updraft and downdraft, and high turbulence in the eyewall of the typhoon.
34 The weather radar observations indicated occurrence of a waterspout in the vicinity of the
35 typhoon. Additionally, the study evaluates the forecasting performance of the AI-based Pangu-
36 Weather model, and the results highlight its better performance than the global numerical
37 weather prediction models in forecasting tropical cyclones in the region. The documentation of
38 these observations aims to provide valuable references for weather forecasters and stimulate
39 further research on forecasting this type of tropical cyclones.

40

41 **1 Introduction**

42 September and October 2023 were eventful months for the occurrence of weather-related
43 natural hazards over southern China. In early September, the region was affected by Super
44 Typhoon Saola which was a rather small tropical cyclone (TC) yet the second most intense TC
45 affecting the South China Sea since 1950. From the radar pictures of Hong Kong when Saola
46 got close to the territory, the eyewall had a diameter of around 70 km only. Saola's eye further
47 shrank in size when it passed south of Hong Kong. It is a rather special cyclone bringing
48 hurricane force winds to Hong Kong and the case has been documented in a number of papers,
49 including observational study (Chan et al., 2023a), aircraft data (He et al., 2023), and forecast
50 (Chan et al., 2023b). About a week later, the remnant of TC Haikui brought torrential rain to the
51 Pearl River Estuary and its neighbouring areas. The Hong Kong Observatory (HKO) registered
52 a record-breaking hourly rainfall of 158.1 millimetres ending midnight on 7 September 2023
53 since records began in 1884. It led to serious flooding at a number of places in Hong Kong.

54 On the evening of 8 October 2023, Severe Typhoon Koinu, surprisingly took on a
55 northerly track towards Hong Kong for a few hours when it was located to the coastal waters
56 south of the territory. In view of public safety, the Increasing Gale or Storm Signal No. 9 in
57 Hong Kong was issued for the second time of the year. Koinu was even more compact than
58 Saola. From the radar pictures of Hong Kong, its eyewall had a diameter of around 50 km only.
59 However, when being affected by the outer periphery of the eyewall of Koinu, a weather station
60 at around 40 km south of Hong Kong, namely, Huangmao Zhou (HMZ), had registered the wind
61 rising from around 40-50 knots to over 90 knots within an hour only. Winds at HMZ continued
62 to increase afterwards, reaching a peak of around 110 knots. Because of the relatively small size,
63 Koinu was generally poorly captured by the global numerical weather prediction models with a
64 horizontal resolution of the order of 10 km only.

65 To monitor the movement and changes in the wind structure of Koinu, the HKO made
66 use of a variety of measurement platforms, including meteorological aircraft, the newly installed
67 ocean radar, and the newly available synthetic aperture radar (SAR) onboard polar orbiting
68 satellites in real time. This paper summarizes the major observations from these measurements.
69 A waterspout was suspected to occur in the vicinity of the territory in association with Koinu,
70 and observations of which are also included in this paper. Finally there would be a short section
71 on the forecasting aspect of Koinu. It turned out the AI-based Pangu-Weather (Bi et al., 2023)
72 forecasts using deep-learning techniques with different sets of model initial field were capable of
73 forecasting the proximity of Koinu to Hong Kong about 5 days ahead, and as such in medium
74 term (3 to 5 days) the performance of Pangu-based models was generally better than that of the
75 conventional global numerical weather prediction models, which has also been reported for the
76 case of Saola (Chan et al., 2023b). It is hoped that the documented materials would be useful for
77 reference by weather forecasters in the future, and could stimulate further study on forecasting
78 this type of rather special TC in autumn in the northern part of the South China Sea.

79

80 **2 Life history of Koinu**

81 Koinu formed as a tropical depression over the western North Pacific to the east of the
82 Philippines on 29 September 2023. It started to move northwestwards towards the seas east of

83 Taiwan and intensified gradually in the next four days. Koinu intensified into a severe typhoon
84 and reached its peak intensity on 2 October 2023 with a maximum sustained wind of 95 knots
85 near its centre. Koinu turned to move west-southwestwards on 4 October 2023 and weakened
86 into a typhoon after skirting past the southern tip of Taiwan on 5 October 2023. While satellite
87 picture depicted the shrinking of Koinu's circulation, it unexpectedly intensified again into a
88 severe typhoon on 7 October around 200 km southeast of Hong Kong with a maximum sustained
89 wind of 95 knots. Koinu started to drift slowly northwestwards on the afternoon of 7 October
90 2023 and it even took a more northerly track towards Hong Kong on the afternoon of 8 October
91 2023. Koinu came closest to Hong Kong on the night of 8 October 2023 with its centre passing
92 only about 70 km south of the Hong Kong Observatory. It started to move west to west-
93 southwestwards across the western coast of Guangdong afterwards and finally degenerated into
94 an area of low pressure on the night of 9 October 2023.

95

96 **3 Aircraft observations**

97 Three aircraft reconnaissance flights had been conducted for Koinu, namely the morning
98 and evening of 6 October, and the morning of 7 October. Air data probe had collected useful
99 data for these three flights. In particular, for the flight of 7 October, the aircraft was involved in
100 a search and rescue exercise and low level flights had been conducted. For the two flights of 6
101 October, dropsondes had been released near the centre of Koinu.

102 The probe data was collected by the Aircraft Integrated Meteorological Measuring
103 System 20 Hz (AIMMS20), and the descriptions of the system can be found in Beswick et al.
104 (2008) and Chan et al. (2011). The plots of wind data from the aircraft data probe for the three
105 flights are shown in Figure 2. In the first flight, winds were found to be lighter within the eyes
106 and hurricane force winds were found just around the eyewall (Figure 2(a)). In the second flight,
107 the flight pattern was more complex and there was not a clear pattern about the distribution of
108 the winds (Figure 2(b)). Hurricane force winds were found at a limited number of locations
109 only. At that moment, based on the aircraft data, Koinu might be relatively weak.

110 For the third flight, the flight level was lower and widespread hurricane force winds were
111 recorded within the eyewall (Figure 2(c)). This is consistent with the weather radar observation

112 and satellite imagery estimation that Koinu was a severe typhoon. Unfortunately, data were only
113 available at the western half of Koinu so that a full picture of the distribution of winds could not
114 be obtained.

115 Dropsondes were released by the aircraft at a height of approximately 10 km to measure
116 the vertical profiles of wind speed, wind direction, temperature, humidity, and pressure. The
117 descriptions of the dropsondes are provided in Chan et al. (2018) and He et al. (2022). The
118 ASPEN software was used to post-process the dropsonde data (Zhang et al., 2013). The
119 available dropsonde data are analyzed in Figure 3 for radial wind speed, and Figure 4 for
120 equivalent potential temperature. It could be seen from Figure 3 that the boundary layer of
121 Koinu had good inflow, suggesting that Koinu might continue to intensify over the northeastern
122 part of the South China Sea, as indicated by He et al. (2022). On the other hand, the equivalent
123 potential temperature profiles did not show much instability in the atmospheric boundary layer,
124 i.e. the equivalent potential temperatures were generally constant with height and sometimes
125 even increasing with height. According to the results of He et al. (2022), this might suggest that
126 the atmospheric instability was rather limited to favour further strengthening of Koinu at that
127 moment. The filled contour plots of equivalent potential temperature with respect to pressure
128 levels are presented in Figure 5. The warm core structure of the tropical cyclone similar to that
129 shown in Emanuel (2018) is clearly depicted in the figure, which agrees with previous
130 observations (He et al., 2022).

131 The vertical wind speed profiles from dropsondes on 6 October are shown in Figure 6.
132 Similar to previous studies (e.g. He et al., 2022; He et al., 2023), Vickery model provides the
133 best fit for the data points. The wind speed could be as high as around 33 m/s near the surface at
134 a distance of about 24 km from the centre of Koinu.

135 The time series of the various meteorological parameters from the air data probe are
136 shown in Figures 7 and 10 for the flight on the morning of 6 October, Figures 8 and 11 for the
137 flight on the afternoon of 6 October, and Figures 9 and 12 for the flight on the morning of 7
138 October. The calculation of the turbulent kinetic energy (TKE) and eddy dissipation rate (EDR,
139 ϵ) generally follow those in Zhang et al. (2011), Zhao et al. (2019), and He et al. (2023). Below
140 are some observations in general: (a) in crossing/proximity of the eye of Koinu, the wind
141 directions generally went through a circle and the wind speeds were rather low; (b) near the eye

142 of Koinu, the vertical velocity showed much fluctuations, and it could be both positive and
143 negative, reaching around 5 m/s or more in magnitude; (c) the turbulence intensity parameters,
144 namely, turbulent kinetic energy (TKE) and eddy dissipation rate (EDR), were generally the
145 largest near the centre of Koinu; similar to previous study (He et al., 2023), TKE and EDR are
146 highly correlated with each other. The slope is in the order of 1.6 and the y-intercept is around 4
147 to 6. Based on the limited number of samples collected so far with a restricted number of TCs,
148 these parameters appear to be universal and applicable for the TCs under study.

149

150 **4 Radar observations**

151 The weather radars in Hong Kong well captured the structure of Koinu. From the 3-km
152 height imagery, the eyewall of Koinu showed up very well within the radarscope (Figure 13(a)
153 and Figure 14(a)). They serve as validation reference for testing of the capability of ocean radar
154 in analysing the wind structure of Koinu. The ocean surface wind speed and direction patterns of
155 Koinu corresponding to the time of weather radar imageries are shown in Figures 13(b) and
156 14(b). Although extracting ocean wave parameters from the second-order spectra of sea echoes
157 from ocean radar measurements is very challenging to engineering applications (Barrick, 2008;
158 Liu et al., 2007; Wu et al., 2003), recent advancements in the beam sampling method and
159 retrieval algorithms improved the reliability of the derived wind and waves in TC situations (Li
160 et al., 2012). By comparing ocean radar derived wind field with the weather radar pictures, it
161 could be seen that the ocean radar wind data captured the locations of Koinu's eye very well.
162 The difference in the eye fix was just about 10-20 km. The wind speeds derived from the ocean
163 radar were also generally reasonable, though underestimated as compared with the actual
164 observations.

165 On the morning of 7 October, maximum winds of around 20 m/s were found at a distance
166 of about 24 km (Figure 13(b)) and 30 km from the centre (Figure 14(b)). Both hinted the radius
167 of maximum wind of Koinu was of the order of 20-30 km. On the early morning of 8 October
168 (Figure 14(b)), gale force winds generally prevailed over the measurement domain of the ocean
169 radar. This wind pattern also appeared to be reasonable except that an annular ring of maximum
170 wind speed near the centre of Koinu could not be depicted in the derived field. It is probably due

171 to the compact structure of Koinu and limitations in the scale resolved by the remote sensing
172 technique and the retrieval algorithm.

173 Apart from the surface wind speed, ocean radar derived products also include significant
174 wave height. On the morning of 7 October (Figure 15(a)), higher wave height of around 8 m was
175 found to be associated with the strong south to southeasterly winds. Though actual observations
176 are not available, such a pattern also appears to be reasonable. On the morning of 8 October
177 (Figure 15(b)), the wave heights were generally about 6-8 m in the measurement domain. At
178 both times, the wave heights were much lower (well below 2 m) near the centre of Koinu
179 because of weaker winds. This is also reasonable.

180 As in the case of Saola (He et al., 2023), eddy dissipation rate (EDR) map could be
181 obtained from the spectral width data of the weather radars. A sample EDR map is shown in
182 Figure 16. Compared to Saola, this time the EDR is much lower, in the order of 0.3 to 0.35 at
183 most. The turbulence was much lower on the eastern and southern parts of the rainband
184 wrapping into the centre of Koinu.

185

186 **5 Satellite observations**

187 A SAR picture has been obtained when Koinu was located just to the south of Hong
188 Kong. From Figure 17, it clearly showed that Koinu was a very compact storm. The SAR winds
189 were directly obtained from the NOAA's STAR SOCD (Satellite Oceanography and
190 Climatology Division) level-2 SAR data download site. The STAR SOCD TC products include
191 the retrieved products from SAR images captured by different satellites, and the image shown in
192 Figure 17 is the scene captured by the Canadian Space Agency's RCM3 (RADARSAT
193 Constellation Mission). The RCM was launched on June 12, 2019, with the three identical
194 satellites working in concert to achieve daily access to 90% of the world's surface. The
195 comparison results could be found in Figure 17. It could be seen that the SAR winds and the
196 buoy winds are well correlated, though the buoy winds are generally lower, because they are 10-
197 minute mean winds whereas the SAR winds are instantaneous. The availability of SAR wind
198 data greatly help the monitoring and provision of warning service for TCs.

199

200 **6 Waterspout**

201 Associated with the outer rainbands of Koinu, an intense radar echo with a maximum
202 reflectivity over 53 dBZ developed near the Dangan islands (about 20 km south of Hong Kong)
203 at about 08:25 UTC on 9 October 2023. It moved west steadily and displayed a comma shape at
204 around 09:13 UTC based on 1.5° PPI scan of the Qiu Yu Tan Weather Radar (QYTWR) in
205 Shenzhen (Figure 18(a)). Doppler wind field from QYTWR showed a velocity couplet of size
206 less than 5 km (Figure 18(b)), suggesting the formation of a waterspout. The maximum
207 reflectivity core was located at a height of around 2.5 km and the maximum radial velocity was
208 above 20 m/s (Figure 18(c)). The vortex tube related to the waterspout reached a height of about
209 2 km. Tracing the radar echo with reflectivity greater than 53 dBz as a proxy of tracking the
210 waterspout, it seemed to have a rather long lifespan of over 3 hours, and the echo finally
211 weakened after around 11:00 UTC that evening. In Hong Kong, waterspout occurred mostly in
212 the summer months from June to August mostly caused by convective weather. The waterspout
213 brewed from the rainbands of Koinu in the month of October was a relatively rare event.

214 The waterspout associated with Koinu can be regarded as a TC spawned tornado.
215 Carroll-Smith et al. (2023) and Edwards (2012) pointed out several factors favourable to the
216 formation of TC tornadoes which were found applicable in this case. These included (i) the
217 waterspout was formed over the northeastern quadrant relative to Koinu's centre due to
218 climatologically enhanced instability and shear in that region, (ii) QYTWR's radar image (left
219 panel of Figure 18(c)) suggested the presence of shallow-topped "miniature" supercell which
220 was typically formed under high shear and helicity environment as well as concentration of
221 buoyancy in the lowest few kilometres above ground, (iii) the presence of baroclinic boundaries
222 (in this case the Dangan islands or broadly speaking the coastal areas of Guangdong) providing
223 stronger horizontal temperature gradient and higher low-level shear for spawning tornado.
224 Further, some of the precursor requirements for tornado touchdowns as mentioned in Schneider
225 et al. (2007) were observed in this case including a hook shape signature in the radar reflectivity
226 image (comma shape in Figure 18(a)) and the presence of a velocity enhancement signature
227 (VES) of 30 kt (15.4 m/s) or greater in the height range of 2 to 4 km (right panel in Figure 18(c)
228 with peak velocity greater than 20 m/s and height above 2 km) which was a stronger indicator of
229 tornadogenesis. While TC-spawned tornado was seldomly observed near the south China coast,
230 the meteorological factors contributing to the formation of waterspout related to Koinu were

231 found consistent with the results of past studies by Carroll-Smith et al. (2023), Schneider et al.
232 (2007) and Edwards (2012).

233

234 **7 Forecasting aspect**

235 Koinu was very compact to be well resolved by the existing global numerical weather
236 prediction models. Despite some early runs of the global models indicated that Koinu might
237 cross the northern part of the South China Sea as a relatively strong TC, most global models
238 subsequently changed their stories on a consensus that Koinu would rapidly weaken over the
239 northeastern part of the South China Sea and quickly dissipate due to intrusion of drier and
240 cooler air of the northeast monsoon. This might have misled operational forecasting and
241 warning services that Koinu might not pose significant threat to the Pearl River Estuary, even as
242 close as a few days before its closest approach. Nevertheless, the Pangu-Weather model
243 persistently forecast that Koinu would continue to track west along the coastal areas of
244 Guangdong and reach the Pearl River Estuary. As a result, they have much better performance
245 in terms of track error, especially in the forecast period of 2 to 5 days, as shown in the time series
246 plots of Figure 19.

247 In addition to Saola, this is the second time that AI-based models outperformed
248 conventional models in forecasting the movement of a midget TC. The mesoscale model TRAM
249 (Zhang et al., 2022) with a horizontal resolution of 9 km also performed much better than global
250 models, in terms of both track forecast (Figure 19) and intensity forecast where multiple runs of
251 TRAMS indicated an intense yet midget Koinu would manage to reach the Pearl River Estuary.
252 This points to the need for improving the performance of global numerical weather prediction
253 models in forecasting the intensity and movement of TCs.

254

255 **8 Conclusions**

256 Koinu was a difficult case for TC warning service due to its compact size and rather
257 erratic movement over coastal waters of Guangdong. This paper documents the weather
258 observations of Koinu from a number of platforms, including aircraft, radar and satellite. It is

259 hoped that the paper could stimulate further study of this case, particularly the possibility of
260 forecasting the compact structure and erratic track of Koinu.

261 The dropsonde data indicated good inflow in the boundary layer, and the Vickery model
262 provided the best fit for wind speed profiles. The warm core structure of the tropical cyclone
263 was clearly depicted, while the equivalent potential temperature profiles showed limited
264 atmospheric instability. The probe data revealed updraft and downdraft up to about 5 m/s, along
265 with high turbulence near the storm center. A correlation between turbulent kinetic energy and
266 eddy dissipation rate was observed. These findings contribute to our understanding of wind and
267 turbulence structure of tropical cyclones.

268 The SAR picture obtained when Koinu was near Hong Kong revealed its compact nature.
269 The SAR winds showed good correlation with buoy winds, albeit slightly lower due to different
270 temporal scales. The weather radar observations suggest the occurrence of a waterspout in the
271 vicinity of Koinu. Typical characteristics of a TC-spawned tornado were displayed, with factors
272 such as enhanced instability and shear, presence of a shallow-topped supercell, and the influence
273 of baroclinic boundaries. The observations align with previous studies on tornado formation in
274 TCs.

275 Koinu's compact size posed challenges for global numerical weather prediction models,
276 leading to inconsistencies in track forecasts. However, the Pangu-Weather model and the
277 mesoscale TRAM model demonstrated better performance in forecasting Koinu's track and
278 intensity. This highlights the importance of enhancing global models for accurate TC intensity
279 and movement predictions.

280 Based on the results so far in the TC season of 2023, AI-based Pangu-Weather models
281 were found to have outperformed the conventional models in forecasting the track and intensity
282 of TCs. Rather urgent need would be required to improve such models in order to provide
283 effective support to the provision of forecast and warning services of TCs in this part of the
284 world.

285

286 **Open Research**

287 Availability Statement

288 The aircraft data used in the study are available at Zenodo via 10.5281/zenodo.10028903

289 Chan, P. W. (2023). Flight data for Severe Typhoon Koinu [Data set]. Zenodo.
290 <https://doi.org/10.5281/zenodo.10028903>

291

292

293 **References**

294 Barrick, D. E. (2008). 30 Years of CMTC and CODAR. Proceedings of the IEEE/OES/CMTC
295 Ninth Working Conference on Current Measurement Technology, 131-136.

296 Beswick, K. M., Gallagher, M. W., Webb, A. R., Norton, E. G., & Perry, F. (2008). Application
297 of the Aventech AIMMS20AQ airborne probe for turbulence measurements during the
298 Convective Storm Initiation Project. *Atmospheric Chemistry and Physics*, 8, 5449-5463.

299 Bi, K., Xie, L., Zhang, H., Chen, X., Gu, X., & Tian, O. (2023). Accurate medium-range global
300 weather forecasting with 3D neural networks. *Nature*, 619, 533–538.
301 <https://doi.org/10.1038/s41586-023-06185-3>

302 Carroll-Smith, D., Green, B. W., Edwards, R., Bai, L., Litta, A. J., Huang, X., Pattie, L.,
303 Overpeck, S., & McCaul Jr. E. W. (2023). Forecasting tropical cyclone tornadoes and
304 impacts: Report from IWTC-X. *Tropical Cyclone Research Review*, 12, 123-135.
305 <https://doi.org/10.1016/j.tcr.2023.06.003>

306 Chan, P. W. (2023). Flight data for Severe Typhoon Koinu [Data set]. Zenodo.
307 <https://doi.org/10.5281/zenodo.10028903>

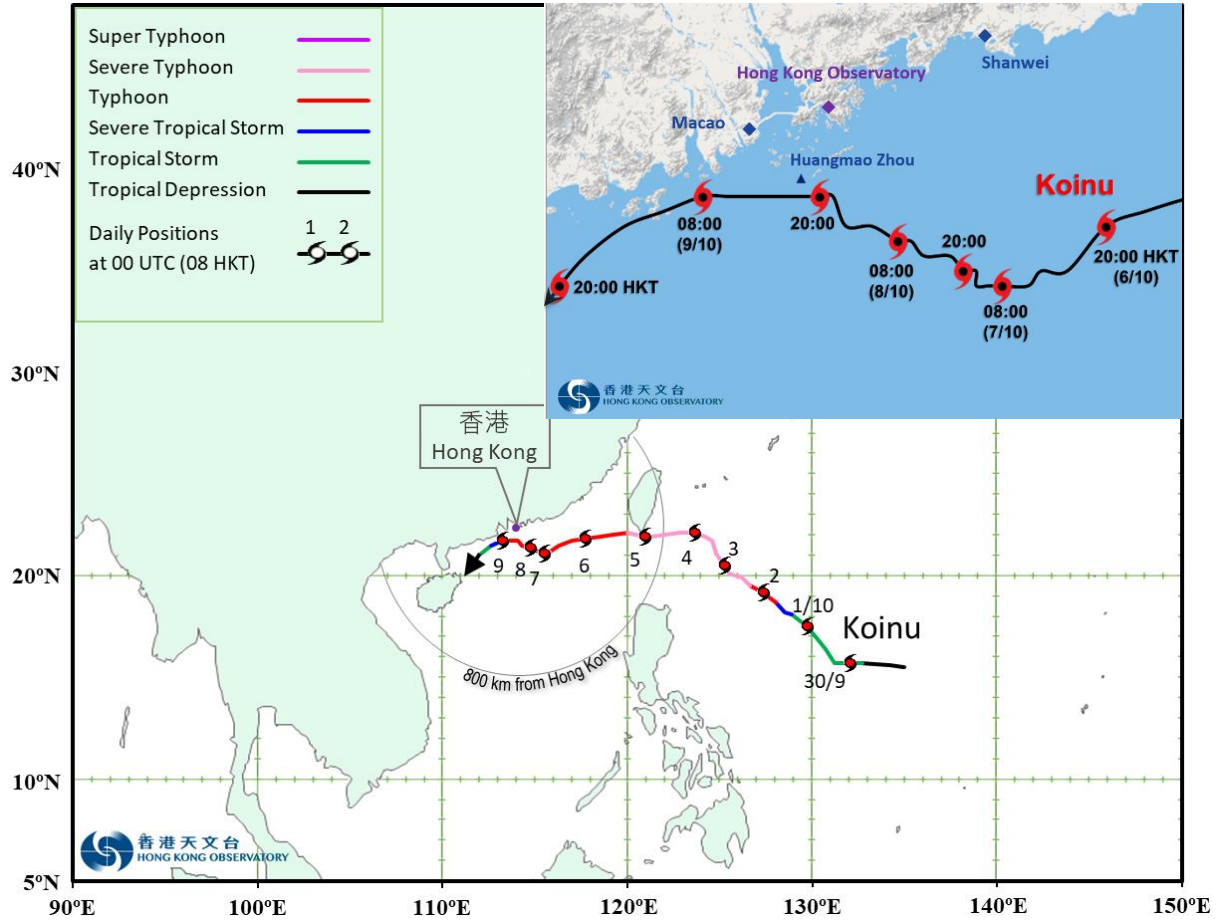
308 Chan, P. W., Choy, C. W., Chiu, Y. Y. (2023a). Observational study of Super Typhoon Saola in
309 2023 when it was close to Hong Kong. *Preprints*, 2023091688.
310 <https://doi.org/10.20944/preprints202309.1688.v1>

311 Chan, P. W., He, Y. H., Lui, Y. S. (2023b). Super Typhoon Saola (2309) affecting Hong Kong in
312 September 2023—Forecasting Aspect. *Preprints*, 2023091634.
313 <https://doi.org/10.20944/preprints202309.1634.v1>

314 Chan, P. W., Hon, K. K., & Foster, S. (2011). Wind data collected by a fixed-wing aircraft in the
315 vicinity of a tropical cyclone over the south China coastal waters. *Meteorologische*
316 *Zeitschrift*, 20, 313-321.

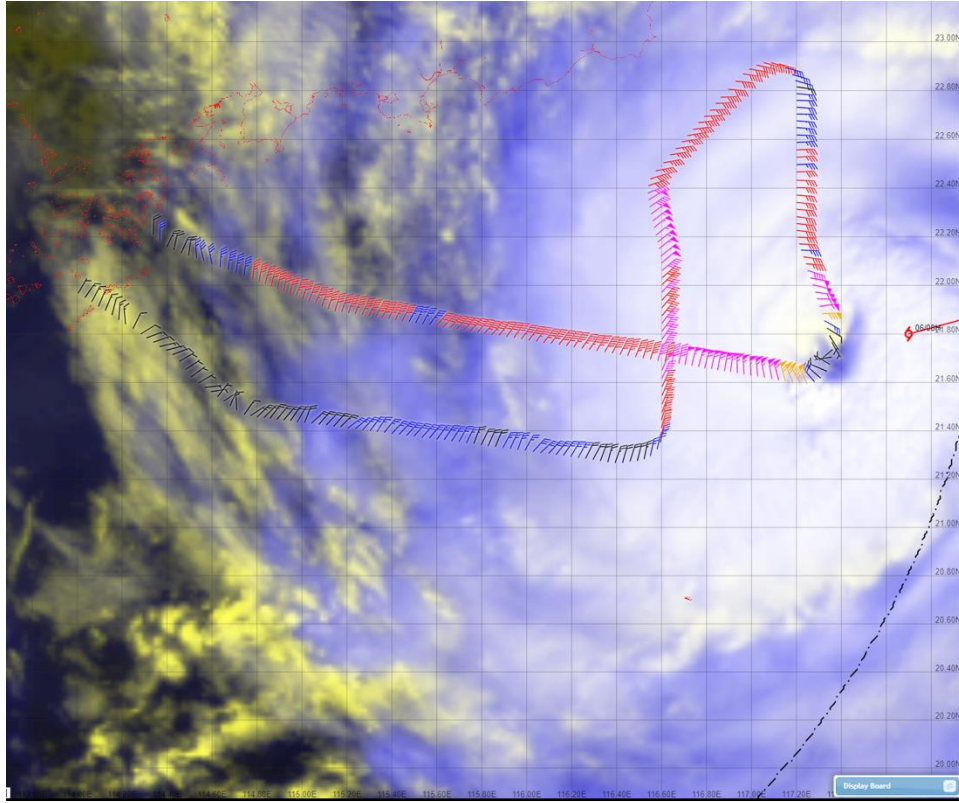
- 317 Chan, P. W., Wu, N. G., Zhang, C. Z., Deng, W. J., & Hon, K. K. (2018). The first complete
318 dropsonde observation of a tropical cyclone over the South China Sea by the Hong Kong
319 Observatory. *Weather*, 73, 227-234.
- 320 Deaves, D. M., & Harris, R. I. (1978). A Mathematical Model of the Structure of Strong Winds,
321 CIRIA Report 76. London, the United Kingdom.
- 322 Edwards, R. (2012). Tropical Cyclone Tornadoes: A review of knowledge in research and
323 prediction. *Electronic Journal of Severe Storms Meteorology*, 7, 1-61.
324 <https://doi.org/10.55599/ejssm.v7i6.42>
- 325 Emanuel, K. (2018). 100 years of progress in tropical cyclone research. *Meteorological*
326 *Monographs*, 59, 15.1-15.68. [https://doi.org/10.1175/AMSMONOGRAPHS-D-18-](https://doi.org/10.1175/AMSMONOGRAPHS-D-18-0016.1)
327 0016.1
- 328 Gryning, S. E., Batchvarova, E., Brümmer, B., Jørgensen, H., & Larsen, S. (2007). On the
329 extension of the wind profile over homogeneous terrain beyond the surface boundary
330 layer. *Boundary-Layer Meteorology*, 124, 251-268. [https://doi.org/10.1007/s10546-007-](https://doi.org/10.1007/s10546-007-9166-9)
331 9166-9
- 332 He, J. Y.; Chan, P.W.; Chan, Y. W.; & Cheung, P. (2023). Super Typhoon Saola (2023) over the
333 northern part of the South China Sea – aircraft data analysis. *Preprints*, 2023091683.
334 <https://doi.org/10.20944/preprints202309.1683.v1>
- 335 He, J. Y., Hon, K. K., Chan, P. W., & Li, Q. S. (2022). Dropsonde observations and numerical
336 simulations for intensifying and weakening tropical cyclones over the northern part of the
337 South China Sea. *Weather*, 77, 332-338. <https://doi.org/10.1002/wea.4123>
- 338 Li, L., Wu, X., Li, Y., Long L., Liu, B., Xu, X., Chen, M., & Xue, C. (2012). Ocean surface wind
339 and wave monitoring at Typhoon Fung-Wong by HFSWR OSMAR071, *Journal of*
340 *Remote Sensing*, 16, 154-159.
- 341 Liu, L., Wu, X. B., Chen, F., Yang, S.L., & Ke, H. Y. (2007). Algorithm for HF radar vector
342 current measurements. *Journal of Oceanography*, 63, 47-66.
343 <https://doi.org/10.1007/s10872-007-0005-x>
- 344 Schneider, D., & Sharp, S. (2007). Radar signatures of tropical cyclone tornadoes in central north
345 Carolina. *Weather and Forecasting*, 22, 278-286. <https://doi.org/10.1175/WAF992.1>

- 346 Vickery, P. J., Wadhera, D., Powell, M. D., & Chen, Y. (2009). A hurricane boundary layer and
347 wind field model for use in engineering applications. *Journal of Applied Meteorology*
348 *and Climatology*, 48, 381-405. <https://doi.org/10.1175/2008JAMC1841.1>
- 349 Wu, X. B., Yang, Z. L., Cheng, F., Wu, Z. C., Yang, Z. J., Wen, B. Y., Shi, Z. F., Tian, J. S.,
350 Hou, J. C., Ke, H. Y., & Gao, H.T. (2003). Ocean surface currents detection at the eastern
351 China sea by HF surface wave radar. *Chinese Journal of Geophysics*, 46, 340-346.
- 352 Zhang, J. A., Marks, F. D., Montgomery, M. T., & Lorsolo, S. (2011). An estimation of turbulent
353 characteristics in the low-level region of intense hurricanes Allen (1980) and Hugo
354 (1989). *Monthly Weather Review*, 139, 1447-1462.
- 355 Zhang, J. A., Rogers, R. F., Reasor, P. D., Uhlhorn, E. W., & Marks, F. D. (2013). Asymmetric
356 hurricane boundary layer structure from dropsonde composites in relation to the
357 environmental vertical wind shear. *Monthly Weather Review*, 141, 3968-3984.
- 358 Zhang, Y., Xu, D., Chen, Z., Meng, W. (2022). Offline diagnostics of skin sea surface
359 temperature from a prognostic scheme and its application in typhoon forecasting using
360 the CMA-TRAMS Model over south China. *Atmosphere*, 13, 1324.
361 <https://doi.org/10.3390/atmos13081324>
- 362 Zhao, Z., Chan, P. W., Wu, N., Zhang, J. A., & Hon, K. K. (2019). Aircraft observations of
363 turbulence characteristics in the tropical cyclone boundary layer. *Boundary-Layer*
364 *Meteorology*, 174, 493-511.
- 365



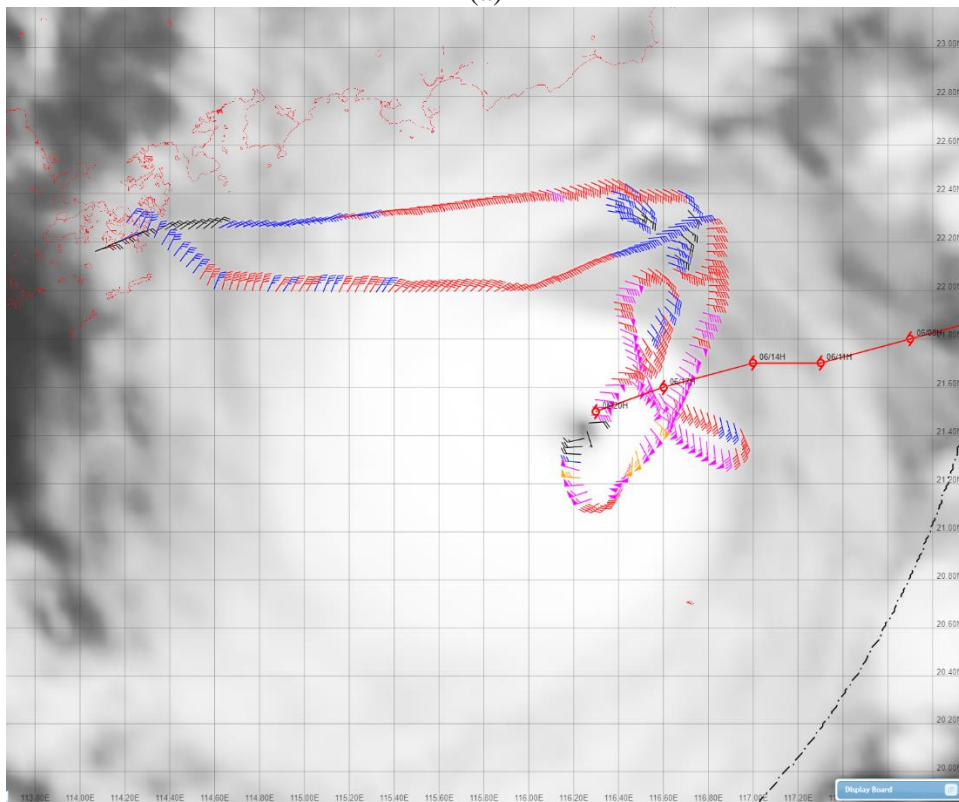
366

367 **Figure 1.** Provisional best track of Koinu and its track near Hong Kong (in Hong Kong Time
 368 (HKT) = UTC + 8 hours). The track of Koinu was slow and erratic during 6 – 8 October 2023.
 369 The centre of Koinu passed very close to Huangmao Zhou on the night of 8 October 2023.
 370



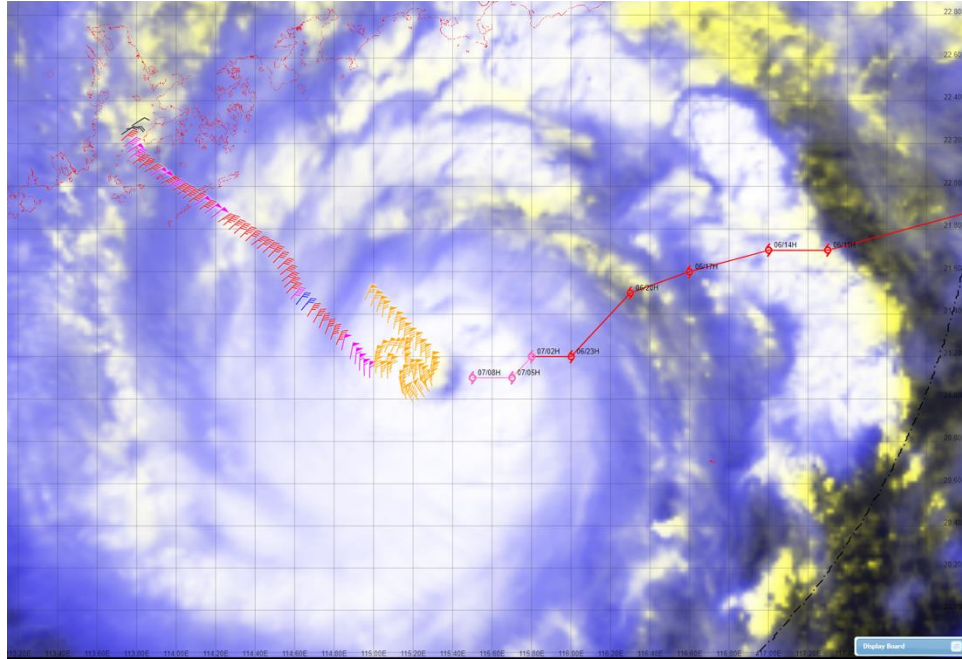
(a)

371
372



(b)

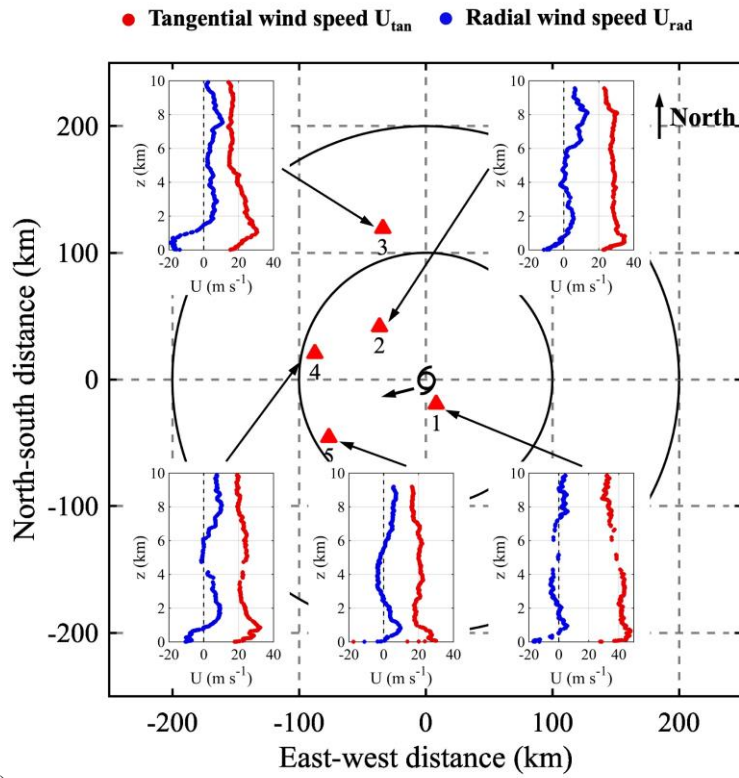
373
374



(c)

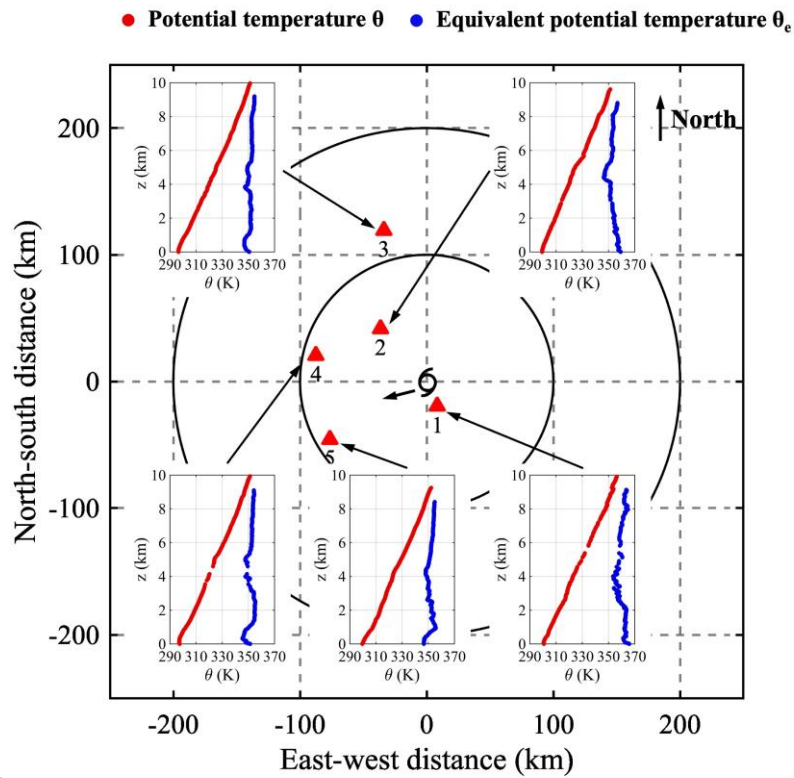
375
376

377 **Figure 2.** Flight routes and selected horizontal wind data along the flights overlaid on images
 378 generated from Himawari-9 geostationary satellite of Japan Meteorological Agency. (a) Flight
 379 between around 02:00 and 03:30 UTC, 6 October 2023 on top of false colour satellite image of
 380 02 UTC; (b) flight between around 11:20 and 13:40 UTC, 6 October 2023 on top of infra-red
 381 satellite image of 12 UTC; and (c) flight between around 01:40 and 02:35 UTC, 7 October 2023,
 382 on top of false colour satellite image of 02 UTC.
 383



384

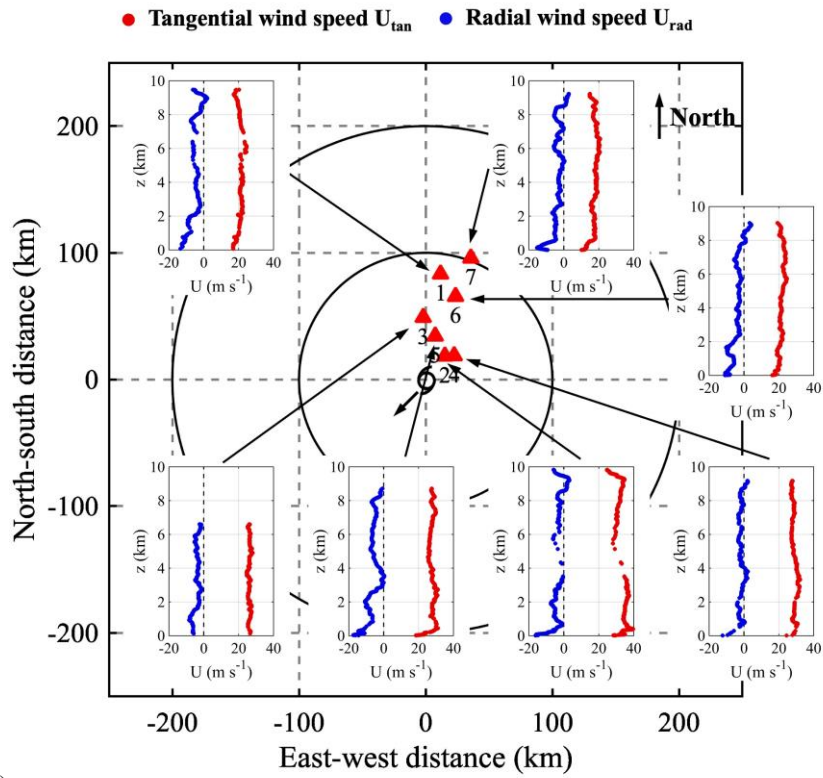
(a)



385

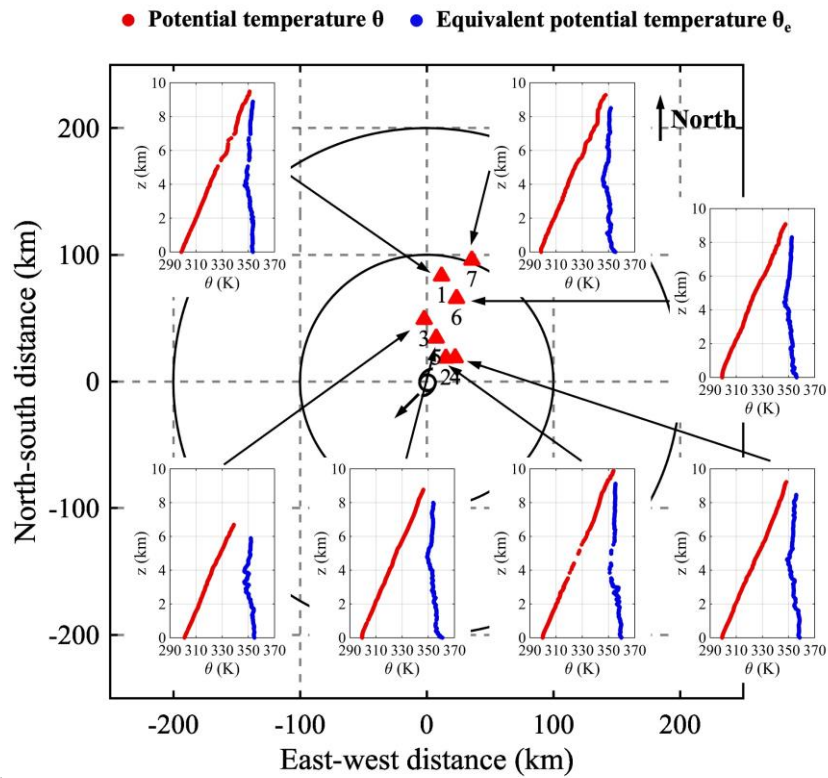
(b)

386 **Figure 3.** (a) Vertical profiles of tangential (red) and radial (blue) wind speeds in Typhoon
387 Koinu at 0300UTC 6 October 2023. Tangential wind speed: anti-clockwise positive; radial wind
388 speed: outflow positive. Red triangles represent dropsonde locations relative to the storm center.
389 (b) Same as (a) but for potential temperature (red) and equivalent potential temperature (blue).
390



391

(a)

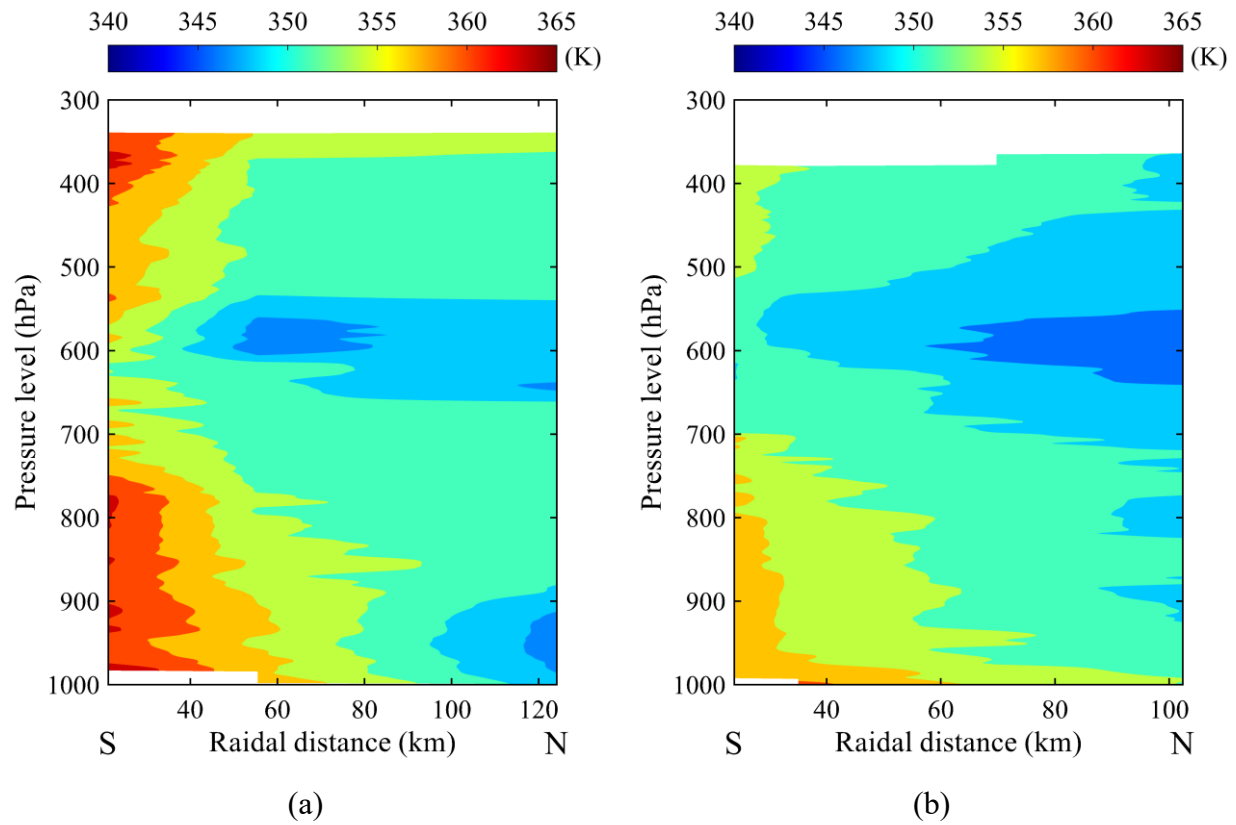


392

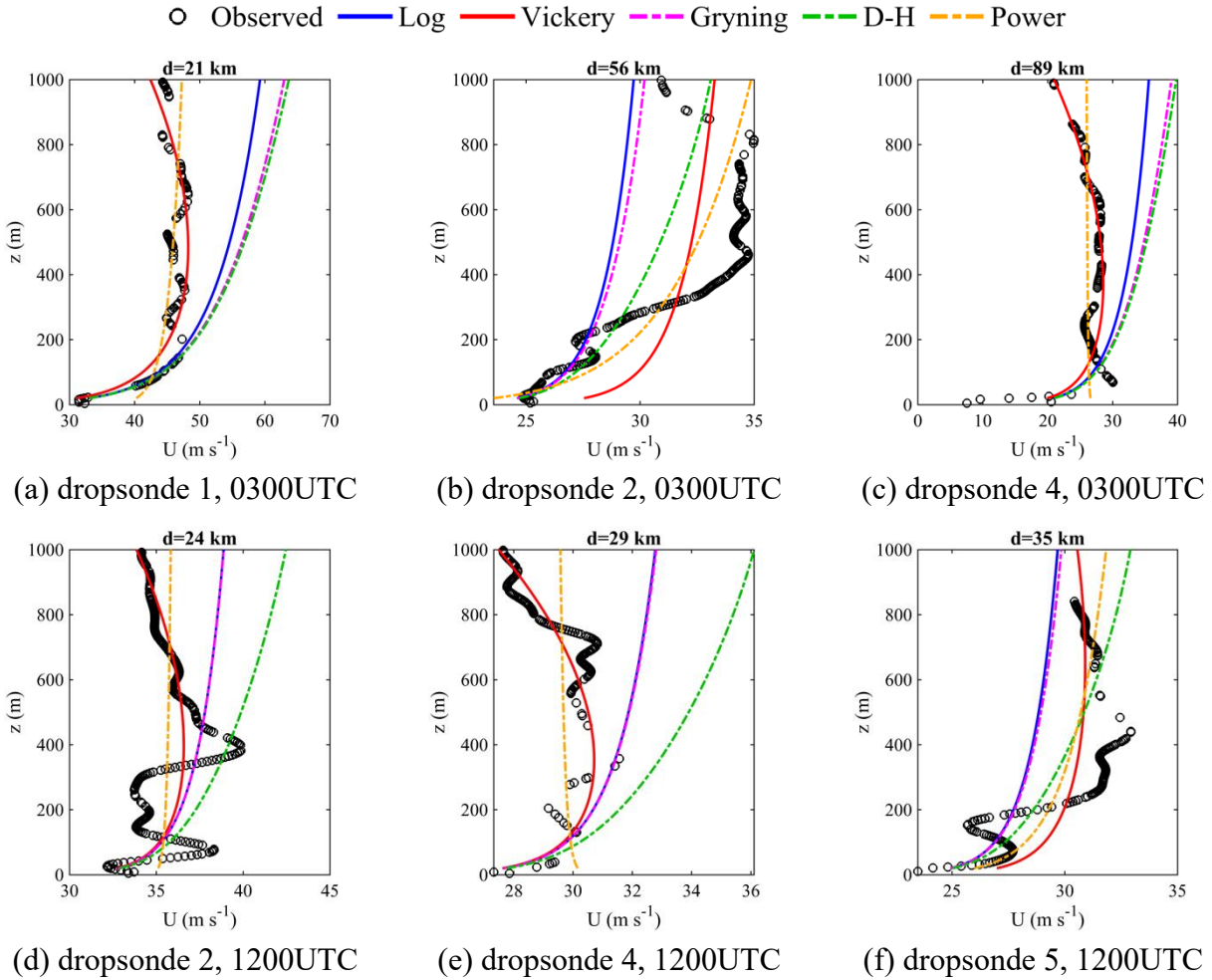
(b)

393
394

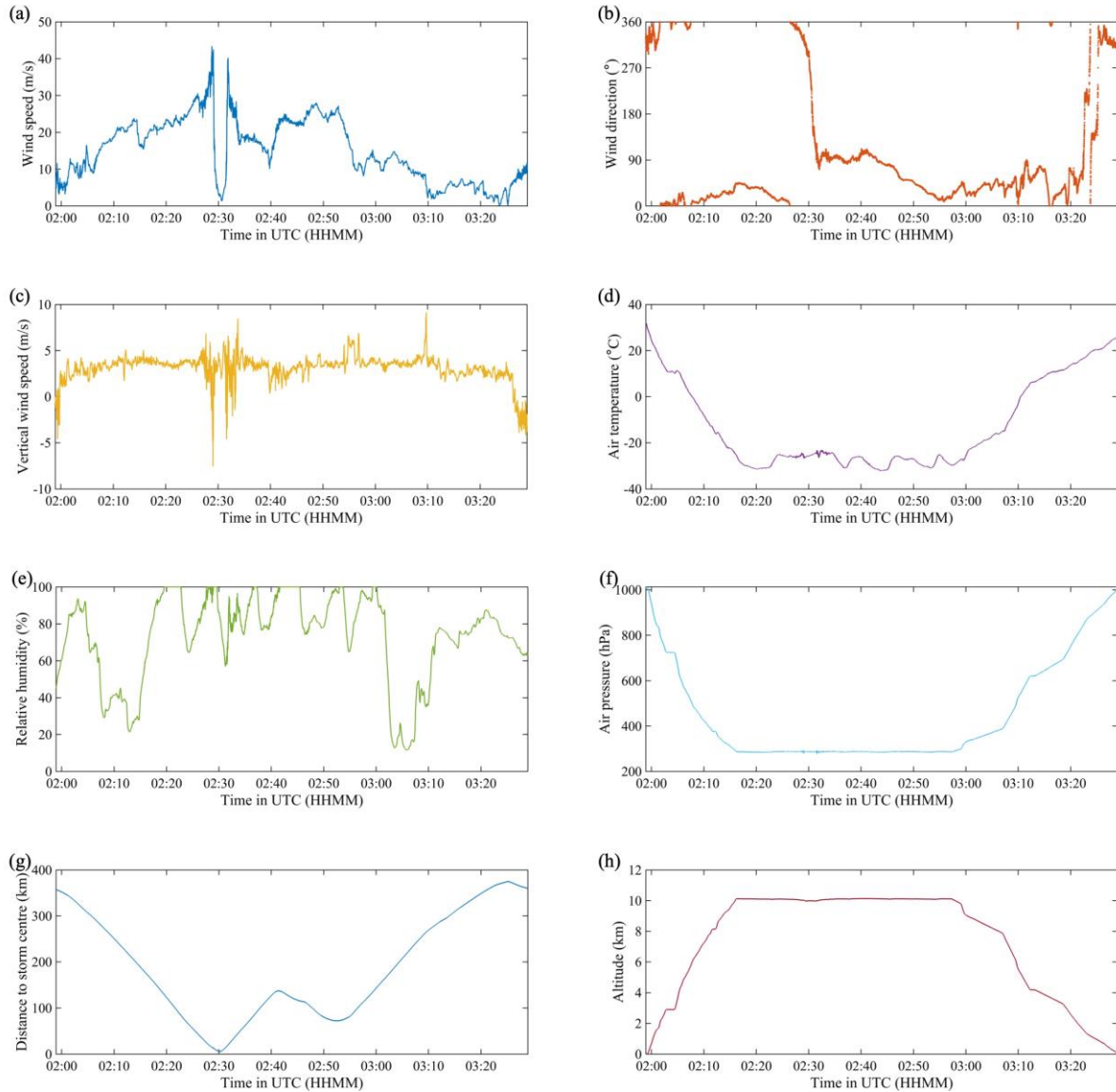
Figure 4. Same as Figure 3 but for observations at 1200UTC 6 October 2023.



395 **Figure 5.** Contour plot of equivalent potential temperature θ_e (in K) in Typhoon Koinu, (a)
396 section observed by dropsondes “1-2-3” at 0300UTC 6 October 2023, and (b) section observed
397 by dropsondes “2-5-6-7” at 1200UTC 6 October 2023.
398

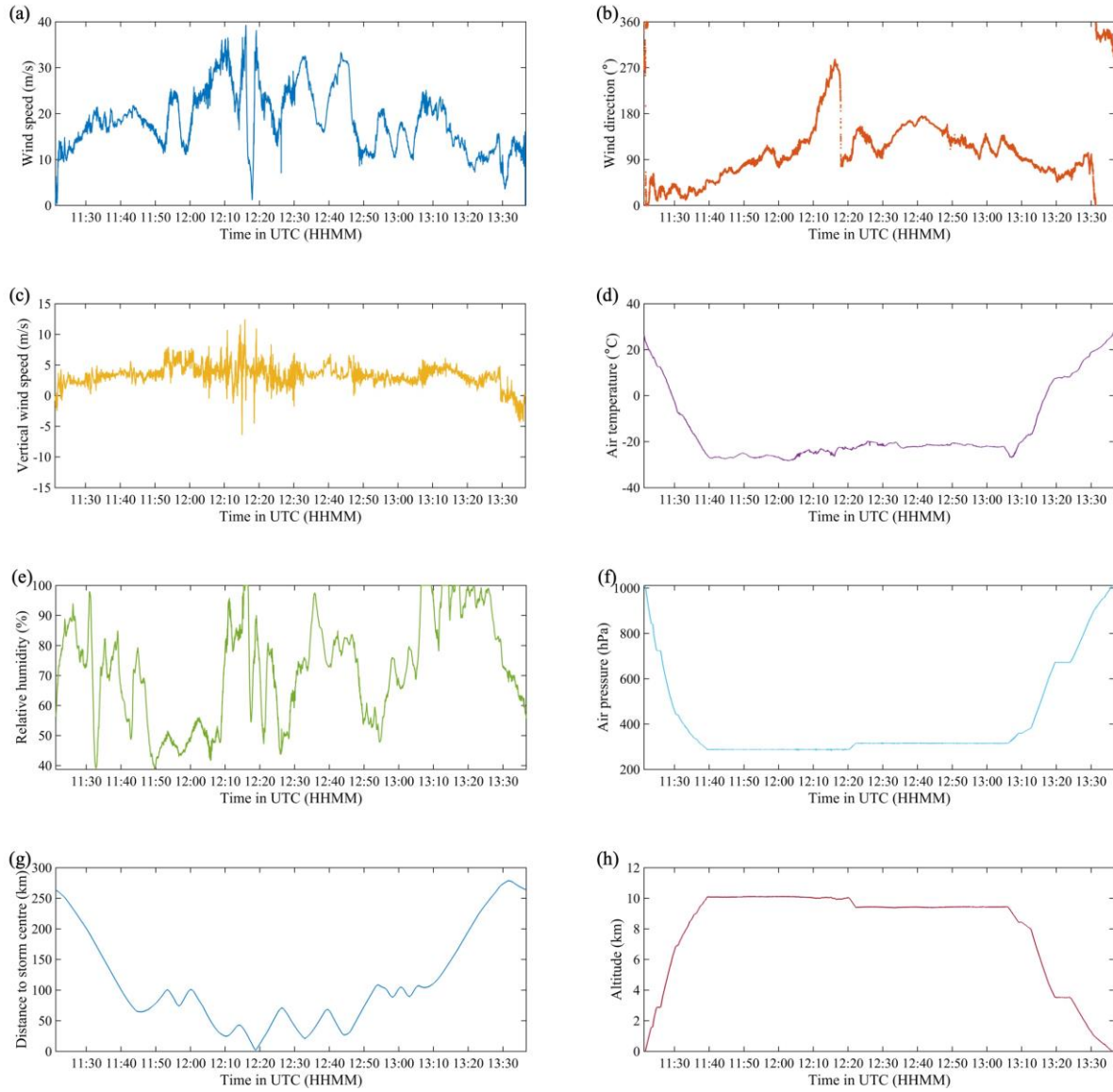


399 **Figure 6.** Fitting of vertical profiles of wind speeds in the lowest 1000 m in Typhoon Koinu to
 400 the wind profile models, including the logarithmic law, Vickery et al. (2009) model, Gryning et
 401 al. (2007) model, Deaves & Harris (1978) model, and power law, (a-c) at 0300UTC 6 October
 402 2023 and (d-f) at 1200UTC 6 October 2023. d represents the distance to the storm center..
 403



404

405 **Figure 7.** Time series of the (a) wind speed, (b) wind direction, (c) vertical wind speed, (d) air
 406 temperature, (e) relative humidity, (f) air pressure, (g) flight altitude, and (h) distance to storm
 407 centre based on the aircraft data in Typhoon Koinu between 0200 and 0330UTC 6 October 2023.
 408

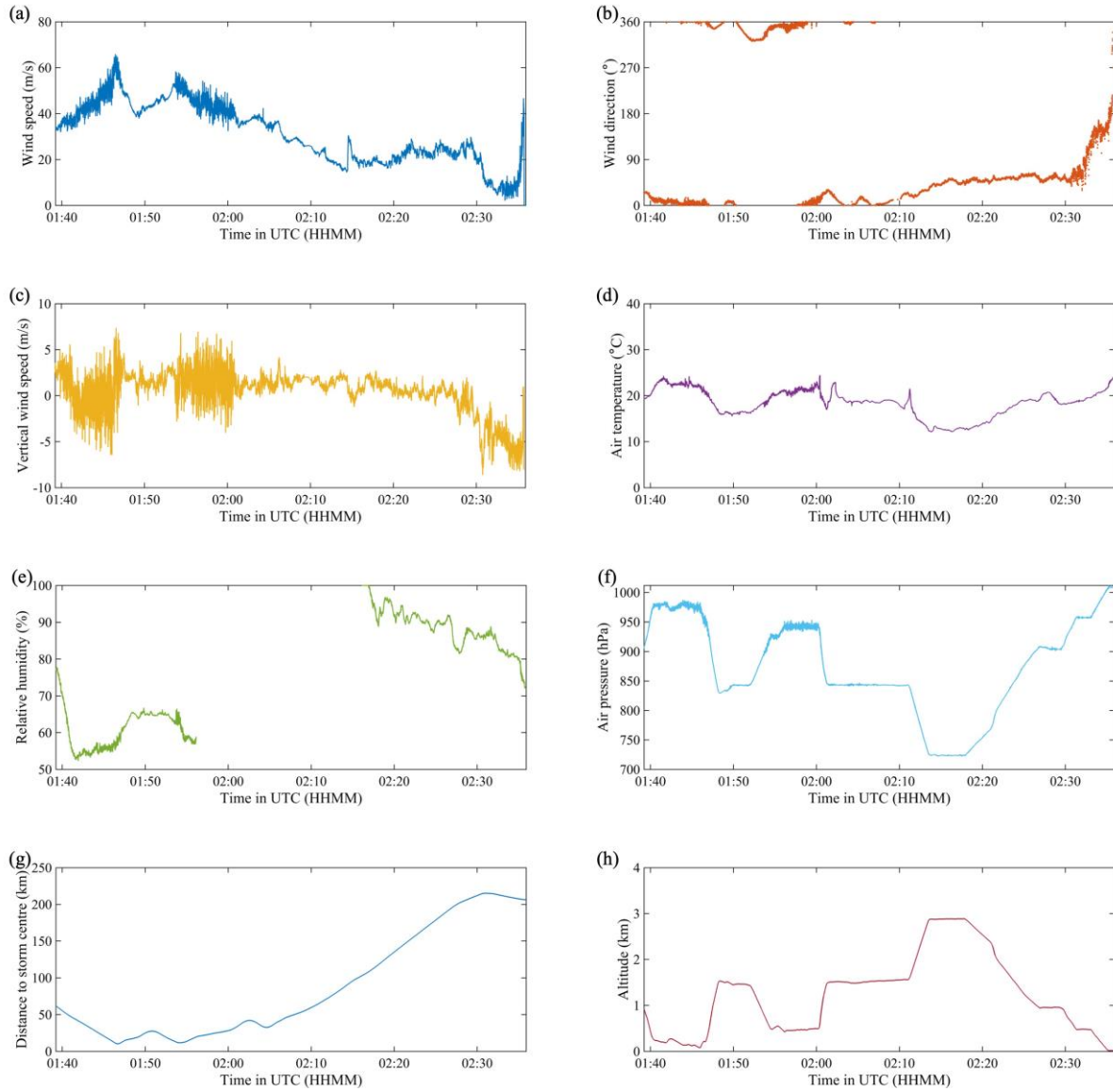


409

410

411

Figure 8. Same as Figure 7 but for observations between 1130 and 1330UTC 6 October 2023.

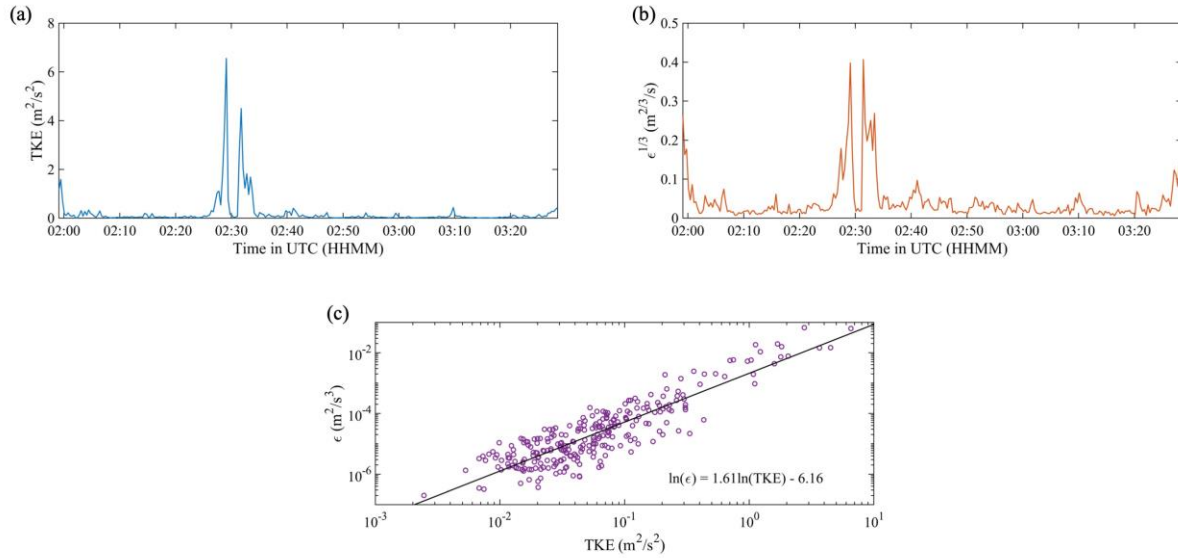


412

413 **Figure 9.** Same as Figure 7 but for observations between 0140 and 0240UTC 7 October 2023.

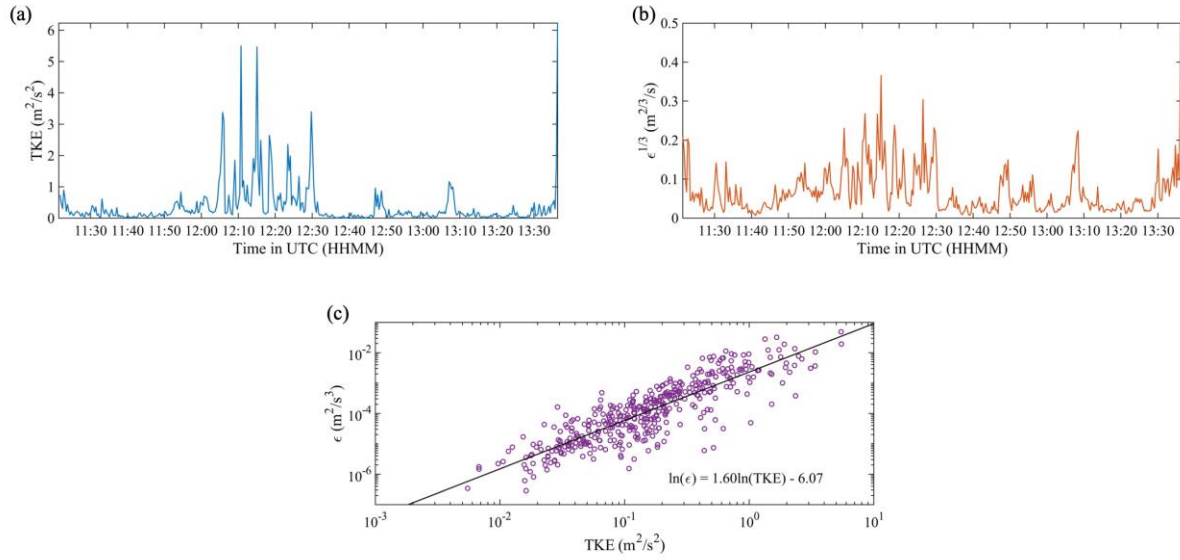
414 The relative humidity data was missing between 0156 and 0215 due to device malfunction.

415



416

417 **Figure 10.** (a) Time series of the turbulent kinetic energy (TKE), (b) time series of the cube root
 418 of the eddy dissipation rate ($\epsilon^{1/3}$), and (c) variation of ϵ with TKE, based on the aircraft data in
 419 Typhoon Koinu between 0200 and 0330UTC 6 October 2023. The black line in (c) represents the
 420 linear fit between $\ln(\epsilon)$ and $\ln(\text{TKE})$.
 421

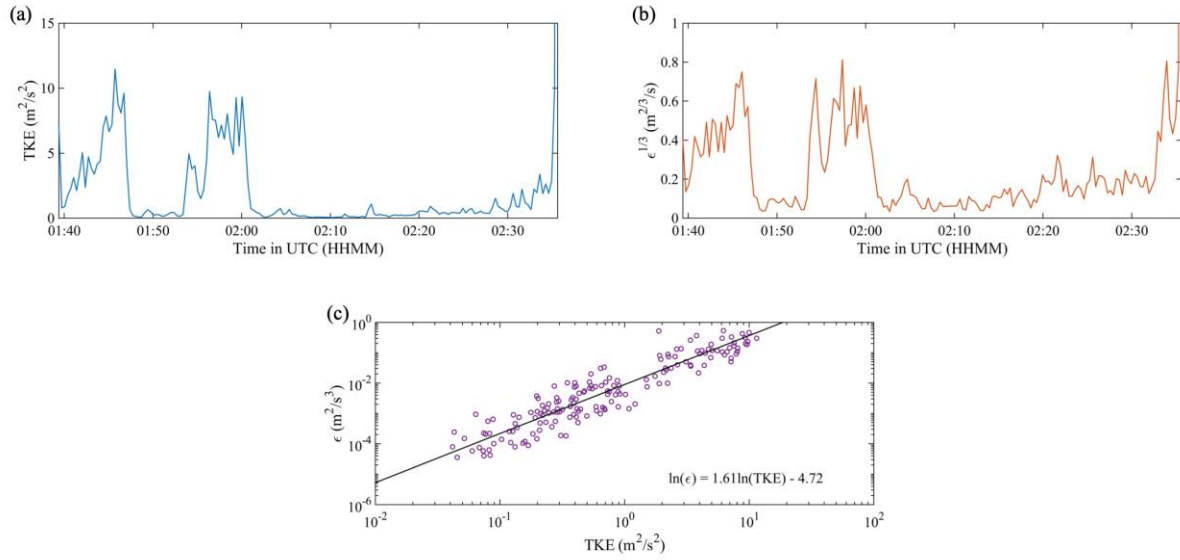


422

423

424

Figure 11. Same as Figure 10 but for observations between 1130 and 1330UTC 6 October 2023.

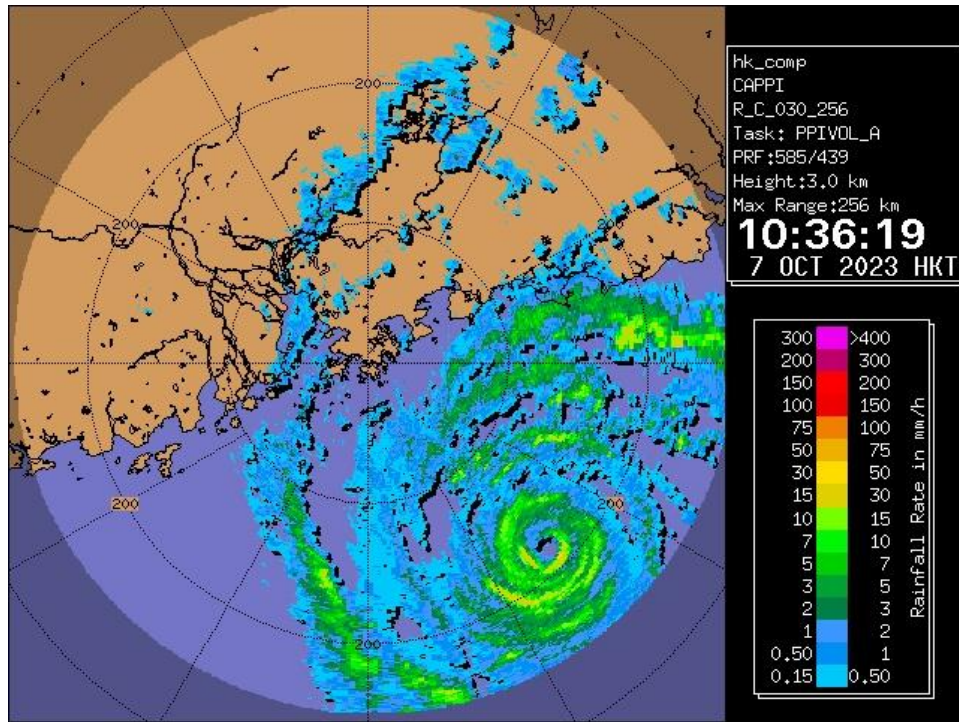


425

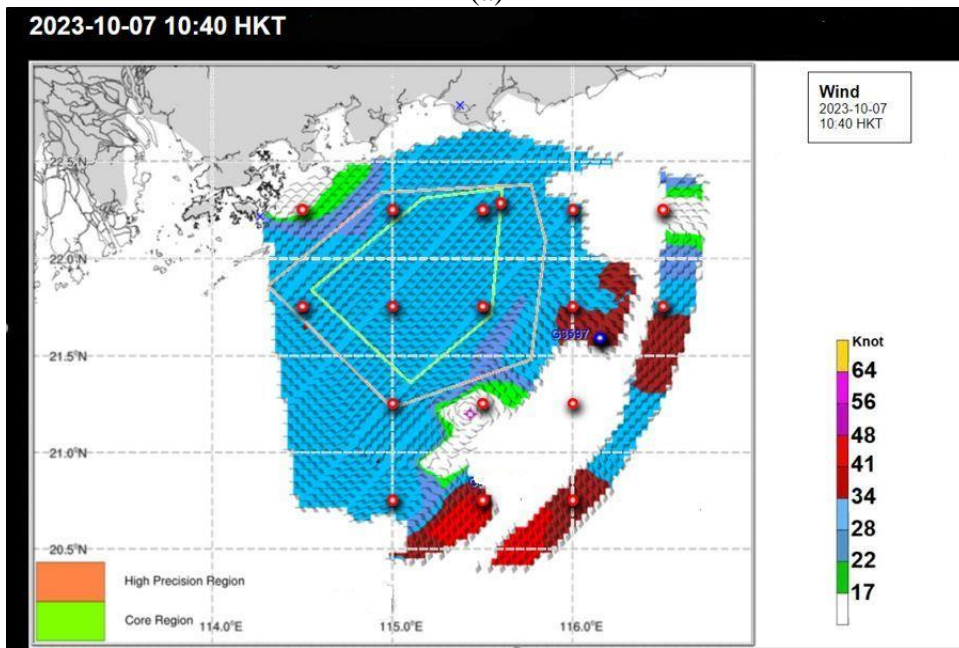
426

427

Figure 12. Same as Figure 10 but for observations between 0140 and 0240UTC 7 October 2023.



(a)

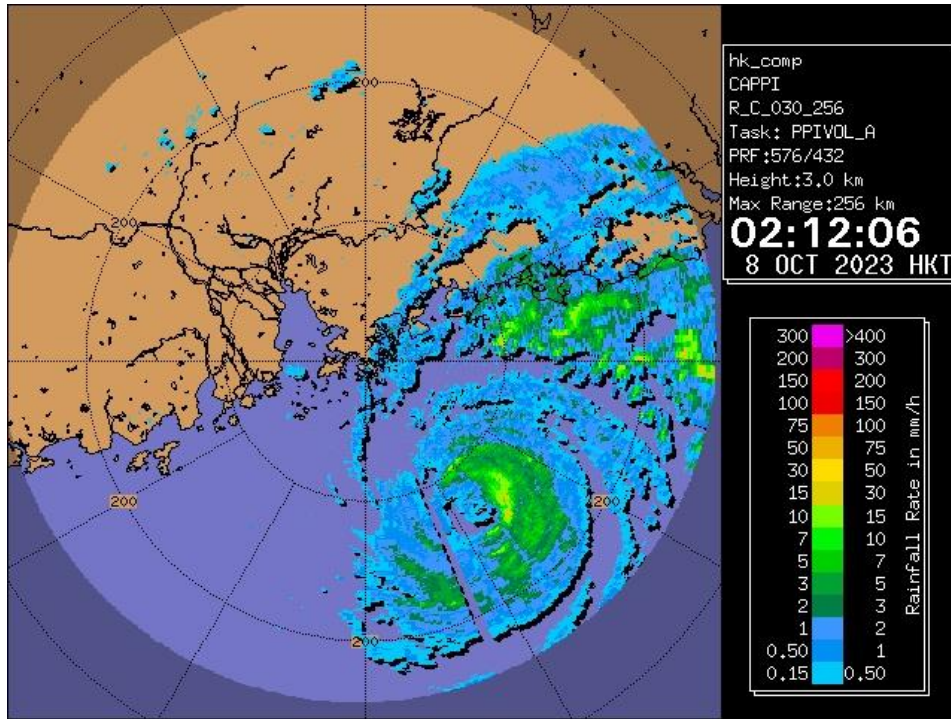


(b)

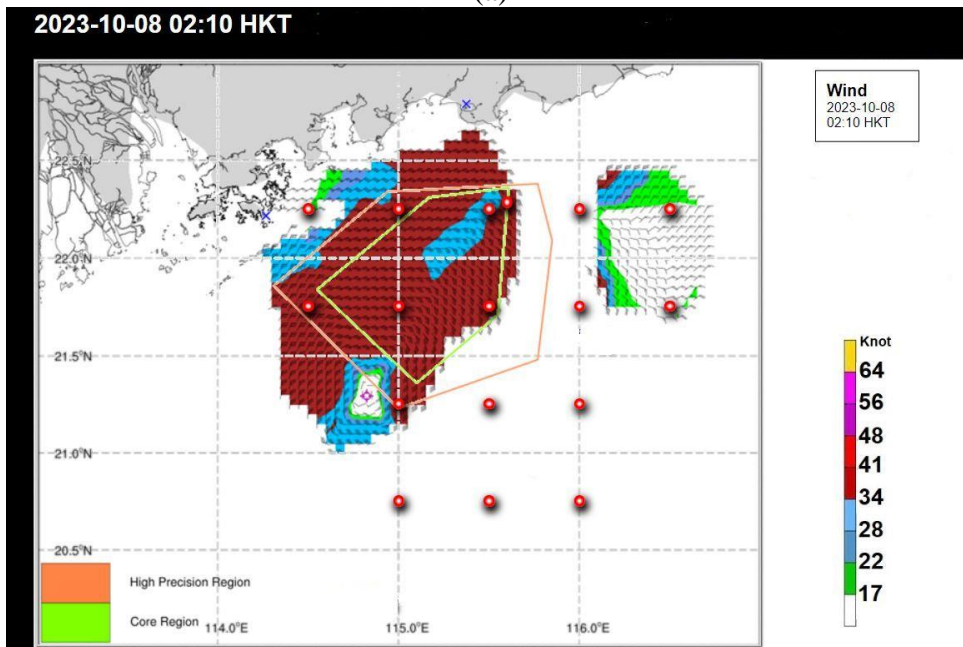
Figure 13. (a) Weather radar imagery at 3-km CAPPI showing Koinu's eye near 21.1N, 115.4E at around 02:36 UTC on 7 October 2023 ; (b) wind field derived from ocean radar around the same time also indicating an eye (purple star) at around 21.2N, 115.4E.

428
429

430
431
432
433
434
435



(a)

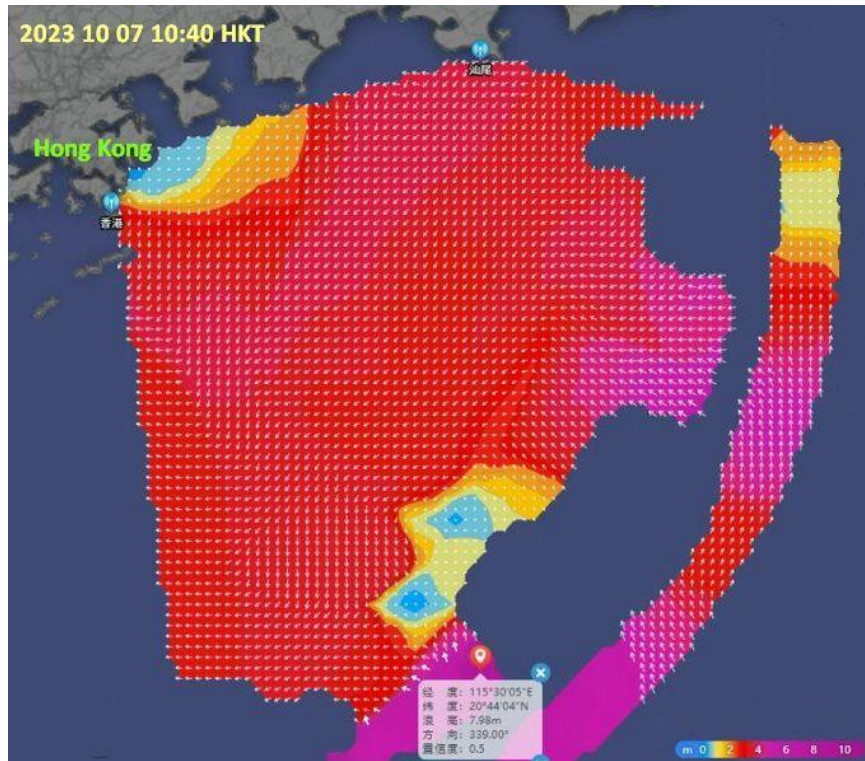


(b)

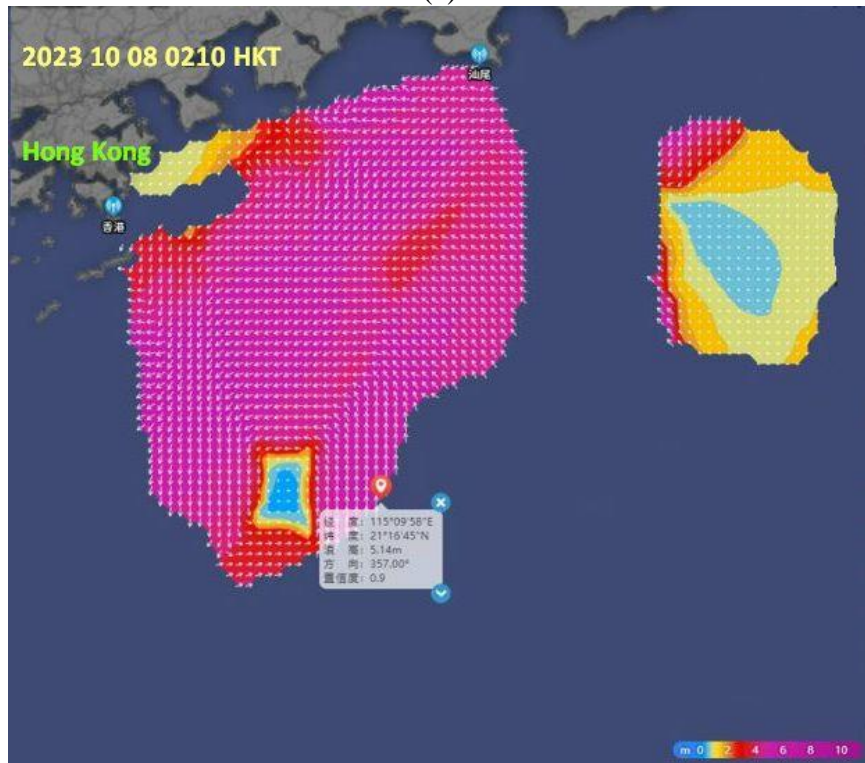
Figure 14. (a) Weather radar imagery at 3-km CAPPI showing Koinu's eye near 21.4N, 115.0E at around 18:12 UTC on 7 October 2023; and (b) wind field derived from ocean radar around the same time also indicating an eye (purple star) at around 21.3N, 114.8E.

436
437

438
439
440
441
442
443



(a)



(b)

444
445

446
447
448
449
450

Figure 15. Significant wave height derived from ocean radar at (a) 02:40 UTC; and (b) 18:10 UTC on 7 October 2023.

20231008 0924HKT 1.0km

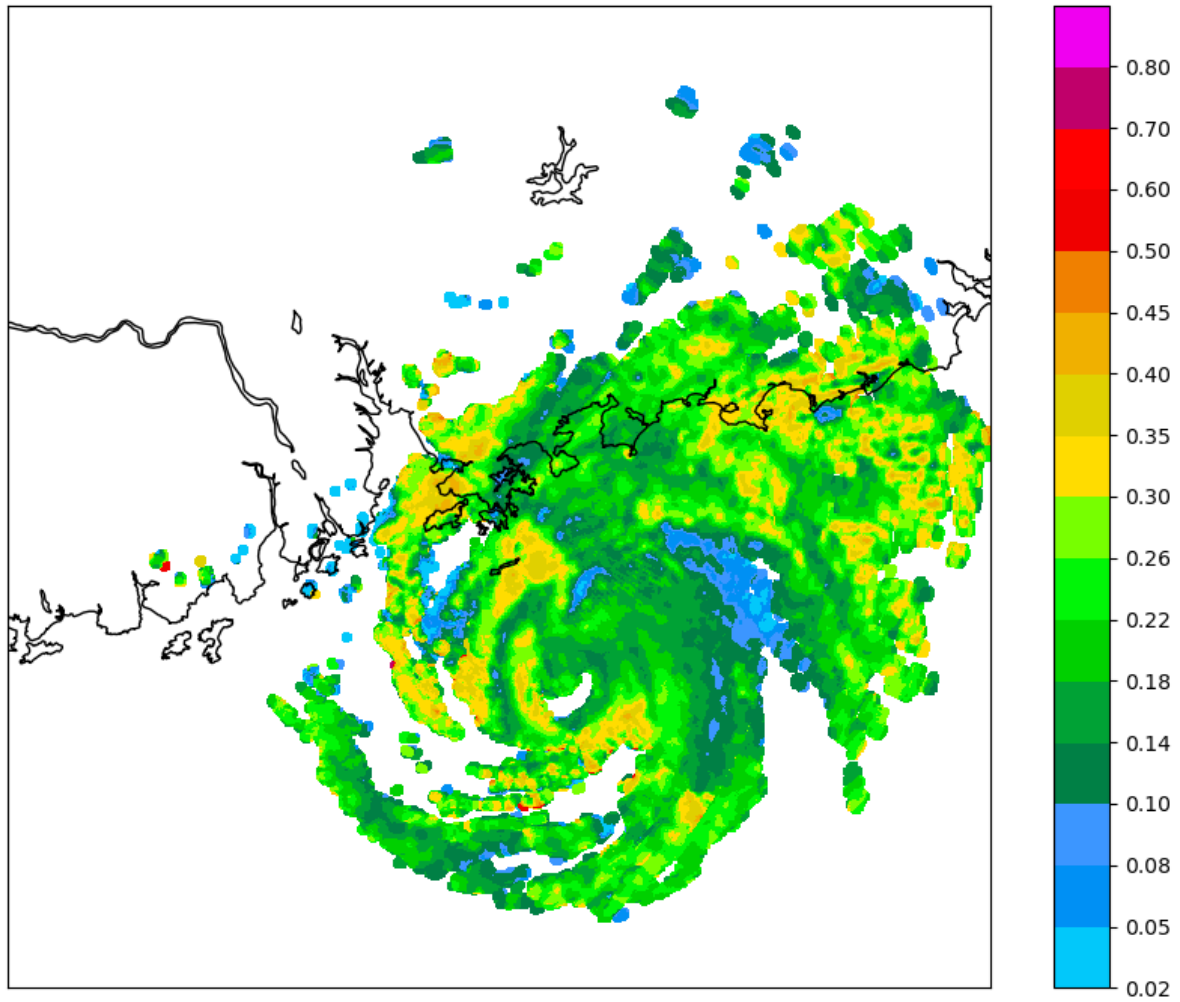
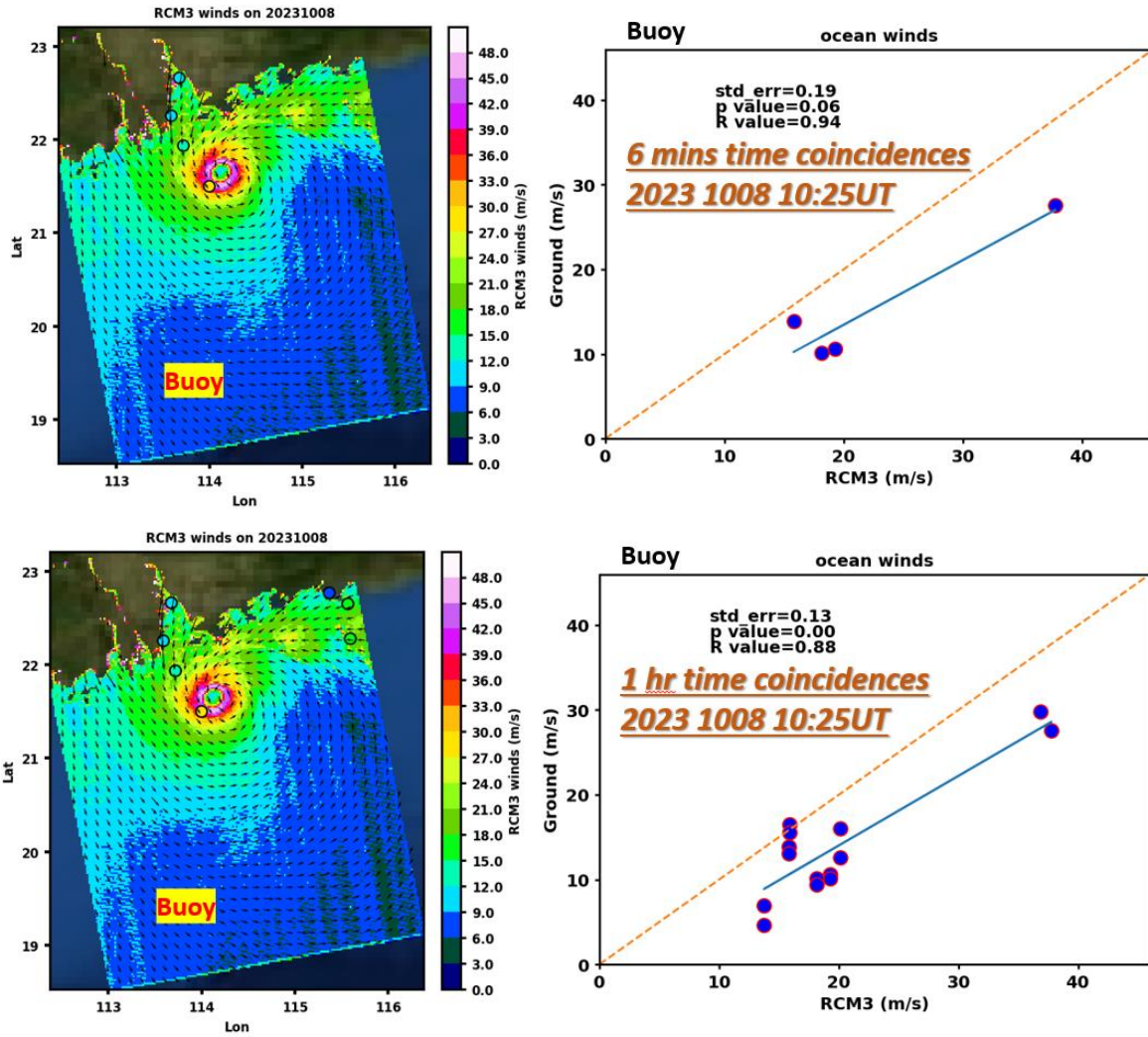


Figure 16. EDR (m^2/s^3) map of Koinu at 01:24 UTC 8 October 2023.

451
452
453

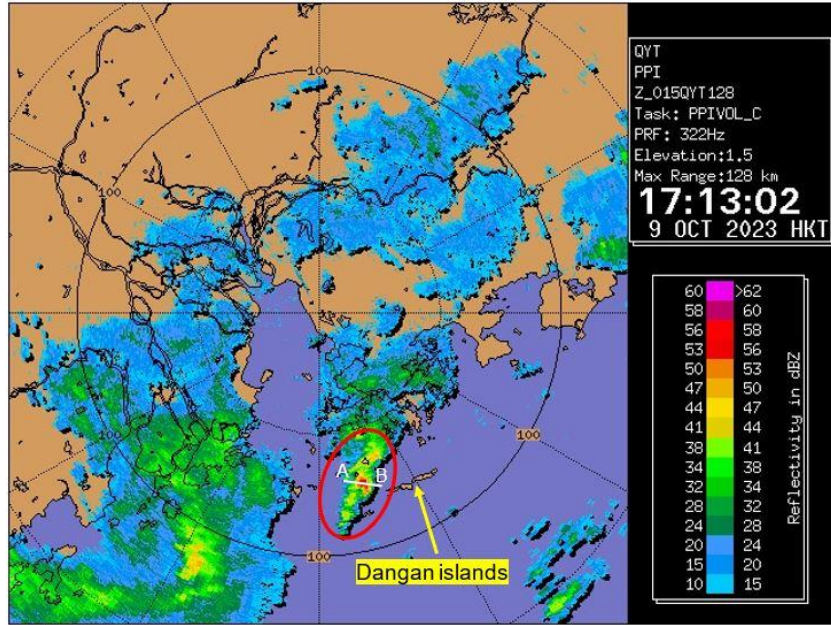


454

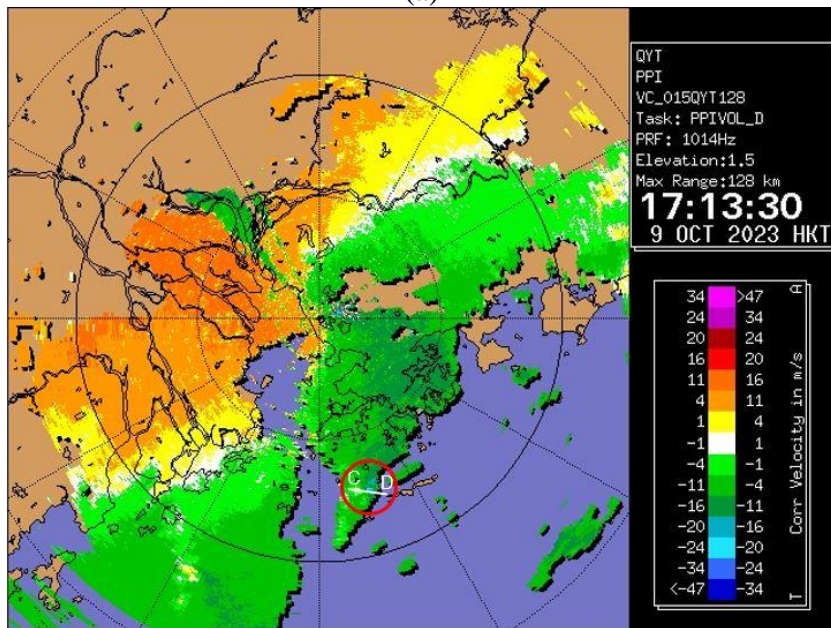
455

456 **Figure 17.** SAR winds captured by Canadian Space Agency's RADARSAT Constellation
 457 Mission (RCM3) on 8 October 2023 (left). Comparison of ocean winds between RCM3 winds
 458 and buoy observations (right).

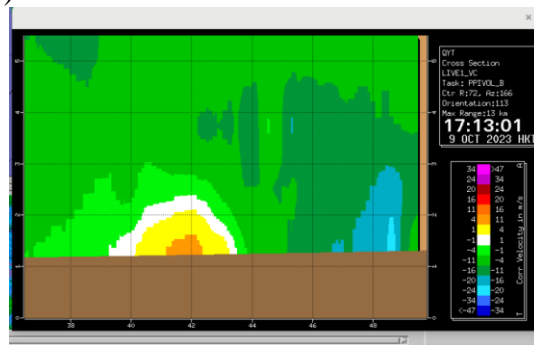
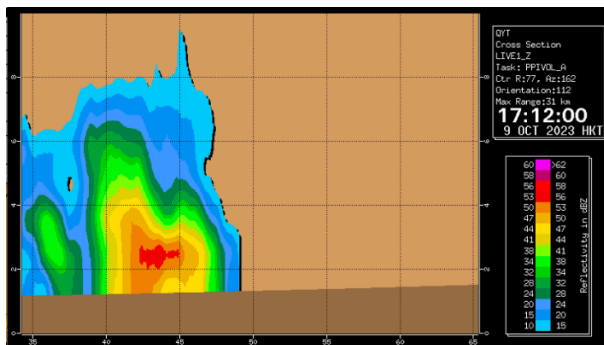
459



(a)



(b)

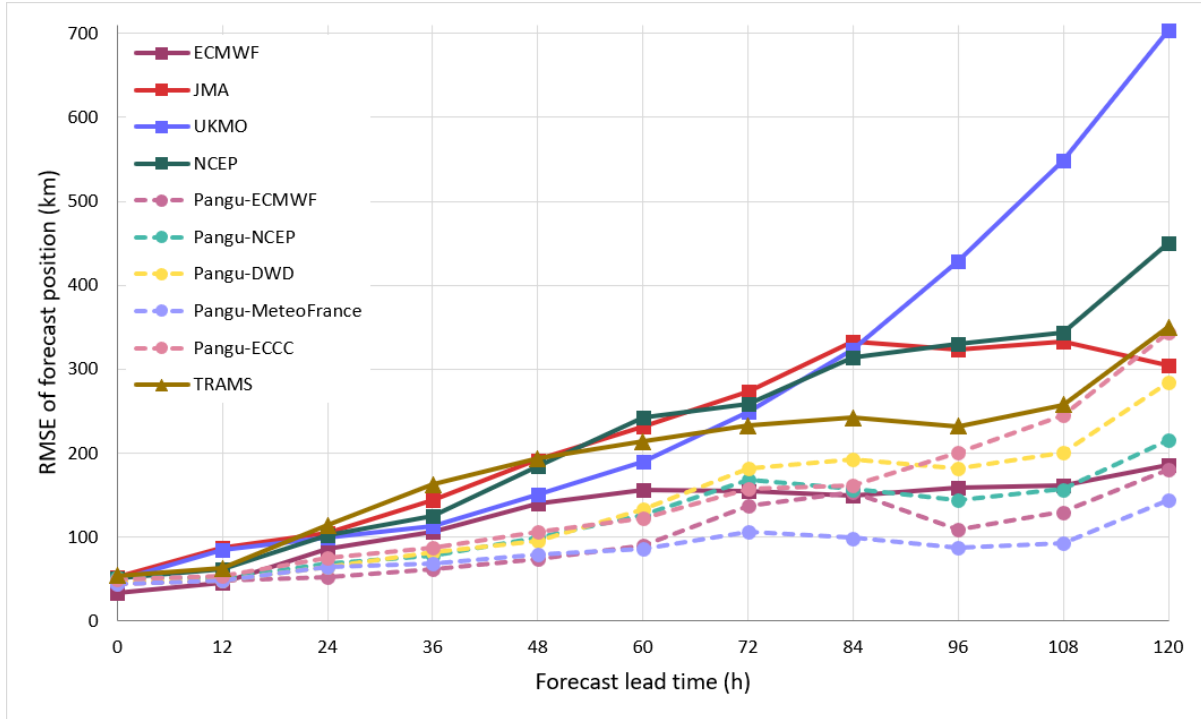


(c)

460
461

462
463

464 **Figure 18.** (a) Reflectivity and (b) radial velocity based on 1.5° PPI scan of the QYTWR at
465 around 09:13 UTC on 9 October 2023. An intense radar echo displaying comma shape (red
466 ellipse) was observed over the seas to the west of the Dangan islands in (a); while a velocity
467 couplet (red ellipse) was observed in (b) in association with the comma shape intense echo in (a).
468 (c) Cross-section along the A-B plane in (a) showing the maximum reflectivity core located at
469 height of around 2.5 km (left panel); while the cross-section along the C-D plane in (b) showing
470 the maximum velocity of the waterspout reaching above 20 m/s with height around 2 km (right
471 panel).
472



473
 474 **Figure 19.** Root-mean-square error of model forecast positions of Koinu as a function of forecast
 475 hours. Forecasts are verified against Koinu’s analysis positions based on HKO’s operational
 476 warning track, and homogenized to have a common data set among different models. Dashed
 477 lines are verification results of forecasts from Pangu-Weather initialized respectively with the
 478 operational analyses of DWD, ECCC, ECMWF, MeteoFrance and NCEP models.
 479